



Tunable Multi-band Switch with Uncoupled Graphene-based Metamaterial Patches

Junjie Zhang^{1,2} · Zheng-Da Hu^{1,3} · Yuxuan Chen¹ · Bolun Zhang¹ · Jicheng Wang^{1,2}

Received: 5 April 2022 / Accepted: 5 June 2022 / Published online: 18 June 2022
© The Author(s), under exclusive licence to Springer Science+Business Media, LLC, part of Springer Nature 2022

Abstract

We present the tunable multiple plasmon-induced transparency (PIT) in the terahertz region by using a metamaterial made of two graphene bands and a graphene square ring. As the different modes of multiple PIT effects are independent of each other, the physical mechanism behind multiple PIT effects can be revealed by CMT theory. The PIT window changes significantly with the Fermi energy levels and structural parameters of graphene. The both three resonant frequencies increase linearly with the parameters and the Fermi energy changing, which can exhibit high sensitivities and figure of merit (FOM). Meanwhile, the amplitude modulation system can reach 99.63%, which can achieve excellent photoelectric switching. In addition, the group index can be as high as 2739. Therefore, the graphene-based metamaterial could be widely used in switches, modulators, excellent slow-light functional devices and filters in the terahertz region.

Keywords Metamaterials · Graphene superstructure surface · Finite element method · Coupled-mode theory · Electro-optical switch

Introduction

For the past few years, metamaterials [1–3], as a material composed of synthetic subwavelength unit cells, have played an increasingly important role in the field of micro-nano-optics. Metamaterials have unique physical and chemical structures and excellent optical, electronic and electrochemical properties that can produce significant interactions with light. Two-dimensional materials including graphene, transitional metal dichalcogenides (TMDs), topological insulators, black phosphorus and Mxene have become hot research topics in the field of metamaterials. Graphene [4–6], made of carbon atoms, has become one of the most important research directions in the field of metamaterials because of its high electron mobility [7, 8], controllable

optical properties [9], and electrical tunability [10, 11]. The Fermi energy of graphene can be easily changed by altering the bias voltage [12, 13], which can change its properties without changing its shape. Therefore, graphene has great potential for realizing tunable devices.

The Fano resonance [14], a special curve asymmetry, is caused by the interaction between the continuous and discrete states. We can achieve Fano resonance through asymmetric graphene structure. The diffraction limit, a phenomenon prevalent in conventional optical devices, can be overcome by Fano resonance in graphene [15]. For this reason, graphene has a very broad application prospect in sensors, nonlinear optics, near field imaging and other fields [16–18]. Plasmon-induced transparency (PIT) [19], a special kind of Fano resonance, is produced by the interaction of superradiant (bright mode) and subradiant modes (dark mode) that can form the absorption peaks and valleys, respectively, in the absorption spectra of the materials [20–22]. The PIT phenomenon will be excited at the same frequency of the two modes. Through scientific research, PIT metamaterials made of monolayer graphene structure and mixed metal-graphene nanostructure can be applied to sensors, modulators and slow light devices [23]. In addition, PIT metamaterials composed of graphene have a strong ability to modulate the resonant frequency of curves,

✉ Jicheng Wang
jcwang@jiangnan.edu.cn

¹ School of Science, Jiangnan University, Wuxi 214122, China

² State Key Laboratory of Applied Optics, Fine Mechanics and Physics, Changchun Institute of Optics, Chinese Academy of Sciences, Changchun 130033, China

³ Key Laboratory of Quantum Information, University of Science and Technology of China, Chinese Academy of Sciences, Hefei 230026, China

so another important application of PIT metamaterials is optical switching. However, most reported graphene structures, due to no independent modulation function for the resonance frequency of PIT curve, cannot meet the requirements of practical applications.

Therefore, we can acquire terahertz optoelectronic devices by combining the optical and electrical properties of graphene with PIT for static and dynamic terahertz tunable devices. Inspired by recent research, a double-layer graphene metamaterial is proposed in this paper, which is made of two covering graphene bands of structural parameters and a lower graphene square ring, which can implement PIT resonance by coupling between different patterns. Unlike traditional single-layer graphene-based optical absorbers, we have designed an independently tunable dual-band absorber consisting of a two-layer graphene stack that does not require the preparation of metal nanostructures. We obtain the PIT projection curve with three resonant frequencies, which can be explained by electrical field distributions, mixing theory and quantum energy level theory, and its transmission spectrum is fitted by coupled mode theory (CMT). In order to better understand the principle behind it, the transmission spectrum of a metamaterial structure is calculated theoretically by using the coupled mode theory, and the theoretical calculation results are in good agreement with the simulation results. Moreover, the resonance frequency of the PIT transmission spectrum obtained by us will change linearly with the change of structural parameters and Fermi energy levels, which indicates that the structure designed by us can be applied to sensors well. Compared to other terahertz modulators, the modulation amplitude of my proposed modulator can reach 99.63%, which means that our modulator can be used as an excellent photoelectric switch. In addition, the group index can be as high as 2739 which means that the graphene-based metamaterial could be widely used in

slow-light function metamaterial. Therefore, we propose a new idea for a terahertz modulator in this paper.

Structure and Theory

The bilayer graphene structure we proposed is shown in Fig. 1a which can show three different resonant frequencies in the band of interest. The geometric parameters of the top and bottom graphene layers are $L_1 = 15.5 \mu\text{m}$ 、 $L_2 = 12 \mu\text{m}$ 、 $L_3 = 2.5 \mu\text{m}$ 、 $L_4 = L_5 = 10.5 \mu\text{m}$ 、 $L_6 = L_7 = 4.5 \mu\text{m}$, respectively. This structure is periodic in the x and y directions with the period $P_x = 20 \mu\text{m}$. The thicknesses of the SiO_2 is $d = 1.2 \mu\text{m}$. The SiO_2 with a refractive index of 1.5 is used as the substrate, and graphene structures are placed on the upper and lower surfaces, respectively, which are divided into upper graphene and lower graphene. The advantage of the two-layer graphene structure is that we can adjust the resonance frequency of the corresponding absorption peak by adjusting one layer individually. By passively adjusting the structural parameters, we can select any number of perfect absorption peaks in a relatively wide terahertz band [5]. The ionic gel layer with a refractive index of 2.5 is wrapped around the graphene pattern. Figure 1b shows the structure we propose which is comprised of two graphene strips with different structural parameters on the upper layer and square ring graphene on the lower layer. In order to better illustrate the different graphene structures, we name the graphene square link, left strip, right strip, left strip and link combination, right strip and link combination as M, L, R, LM and RM, respectively. In this paper, we use COMSOL software to calculate the simulation results of metamaterials including transmission spectrum and electric field distribution. Herein, the structure is illuminated with a monochromatic plane wave propagating along the z -axis and the electric field along the x -axis. In the numerical simulation, the left and right of the

Fig. 1 **a** Schematic diagram of graphene metamaterial on SiO_2 substrate; **b** Top view of metamaterial's structural unit; and size: $L_1 = 15.5 \mu\text{m}$, $L_2 = 12 \mu\text{m}$, $L_3 = 2.5 \mu\text{m}$, $L_4 = L_5 = 10.5 \mu\text{m}$, $L_6 = L_7 = 4.5 \mu\text{m}$, $d = 1.2 \mu\text{m}$, $P_x = 20 \mu\text{m}$

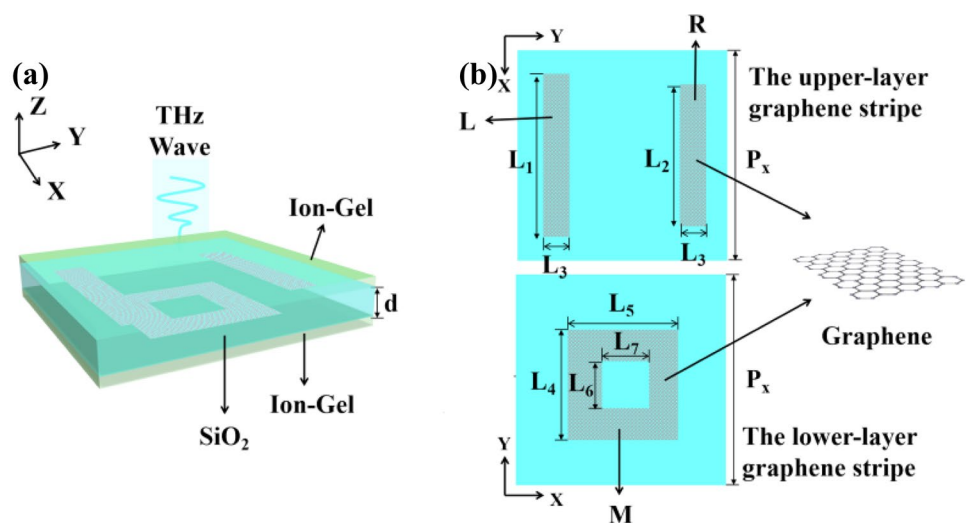
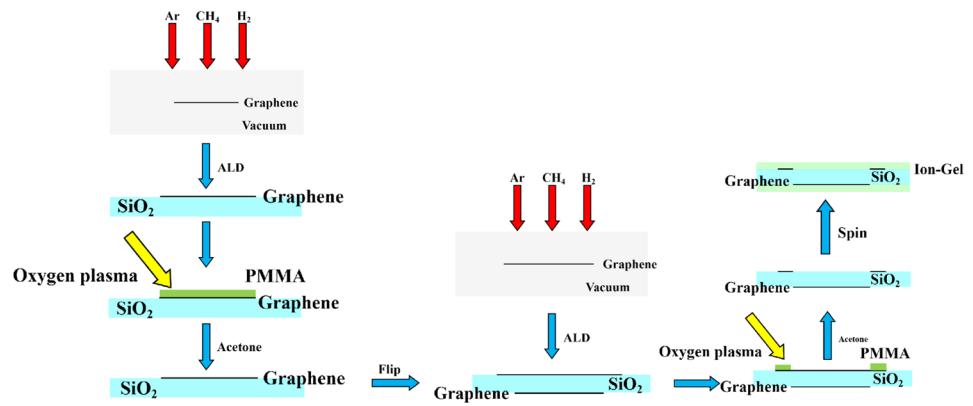


Fig. 2 Process for fabricating the proposed nanostructured metasurfaces



unit cell are set as periodic boundary conditions, and the top and bottom are set as perfect matching layers.

Additionally, the feasibility of experimental fabrication is analyzed. Figure 2 shows the all process flow for fabricating this nanostructure. A continuous, uniform atomic monolayer of graphene was grown by an optimized chemical vapor deposition method using CH₄ as the carbon source and Ar/H₂ as carrier gas. The as-grown graphene was first transferred onto a thin layer of SiO₂—via atomic layer deposition (ALD), then patterned into closely packed nanodisk arrays using e-beam lithography with PMMA as an electron beam resist. Oxygen plasma (40 W, 500 Mt, 15 s.) was used to etch away the exposed area, leaving the periodic pattern of graphene nanodisks protected by a PMMA layer, which was then removed with acetone. The element is then rotated and the upper graphene structure is prepared using the same procedure. To tune the Fermi level of the graphene nanostructure array, a high capacitance ion-gel layer (the physically crosslinked, ionic liquid/triblock copolymer gel) was spin-coated on top of the layer of graphene nanostructures. The ion-gel layer spin-coated onto the graphene pattern was chemically prepared to yield a high capacitance ($C = 2.49 \mu\text{F}/\text{cm}^2$). To prepare the ion gel, 0.56 g of ionic liquid ([EMIM][TFSI]) was first dried under vacuum and then transferred to glove box for 4 days, then it was dissolved with 22 mg of PS-PEO-PS (10–44-10 kg mol⁻¹) triblock copolymer in 2 ml of dry dichloromethane.

Graphene is modeled as a conductive surface by using the transition boundary condition and its thickness is set equal to $t_g = 1 \text{ nm}$. In this paper, on the basis of the Kubo formula, the conductivity formula of monolayer graphene can be indicated as [24, 25]

$$\sigma(\omega) = \frac{2e^2k_B T}{\pi\hbar^2} \frac{i}{\omega + i\tau^{-1}} \ln \left[2 \cosh\left(\frac{E_F}{2k_B T}\right) \right] + \frac{e^2}{4\hbar^2} \left[\frac{1}{2} + \frac{1}{\pi} \arctan\left(\frac{\hbar\omega - 2E_F}{2k_B T}\right) \right] - \frac{e^2}{4\hbar^2} \left[\frac{i}{2\pi} \ln \frac{(\hbar\omega + 2E_F)^2}{(\hbar\omega - 2E_F)^2 + 4(k_B T)^2} \right] \tag{1}$$

where k_B , e , $T = 300 \text{ K}$, \hbar , ω , E_F are the Boltzmann constant, the electron charge, the temperature, the reduced Planck’s constant, the angular frequency of the incident light, and the Fermi energy of graphene.

The carrier relaxation lifetime is showed as $\tau = \mu E_F / e(v_F)^2$, where $v_F = 1 \times 10^6 \text{ m/s}$ defines the Fermi velocity, and $\mu_c = 10000 \text{ cm}^2/(\text{V}\cdot\text{S})$ stands for the carrier mobility. We select $30000 \text{ cm}^2/(\text{V}\cdot\text{S})$ as the carrier mobility which can be high reached $40000 \text{ cm}^2/(\text{V}\cdot\text{S})$ [26] by considering the performance and practical feasibility of our design structure. In the terahertz frequency range ($E_F > \omega$), the formula can be predigested as [27, 28]

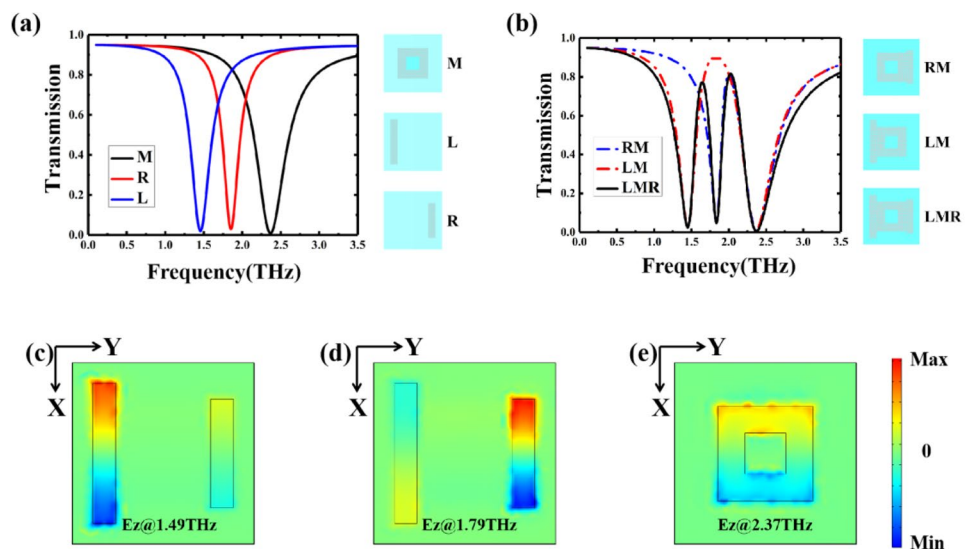
$$\sigma(\omega) = \frac{e^2 E_F}{\pi\hbar^2} \frac{i}{\omega + i\tau^{-1}} \tag{2}$$

We define the effective dielectric constant of graphene as $\epsilon(\omega) = 1 + i\sigma(\omega)/\epsilon_0\omega t_g$ [29] where ϵ_0 is the vacuum dielectric permittivity.

Simulation Results and Discussion

Transmission spectra of the upper-layer and lower-layer structures are shown in Fig. 3a, b. It is observed that L, R and M structures are coupled with incident light at 1.49 THz, 1.65 THz and 2.37 THz, respectively. When L and R structures combine with M structures to form LM and RM structures, LM and RM show single-PIT response, respectively. Finally, we obtain a transmission spectrum with two transparent windows when the M, L and R structures are combined to form the LMR structure. The three components

Fig. 3 **a** Simulated transmission spectra of single M, Single L and single R metamaterials; **b** Simulated transmission spectra of proposed metamaterial LMR, Single LM, and single RM metamaterial structures. Here, Fermi levels of graphene are both 1.2 eV; **c** E_z distribution of three resonant frequencies in the transmission spectrum of the material



of the metamaterials have different resonant frequencies, which causes the frequency asymmetry of the two transparent windows in response to the double pit of the proposed structure.

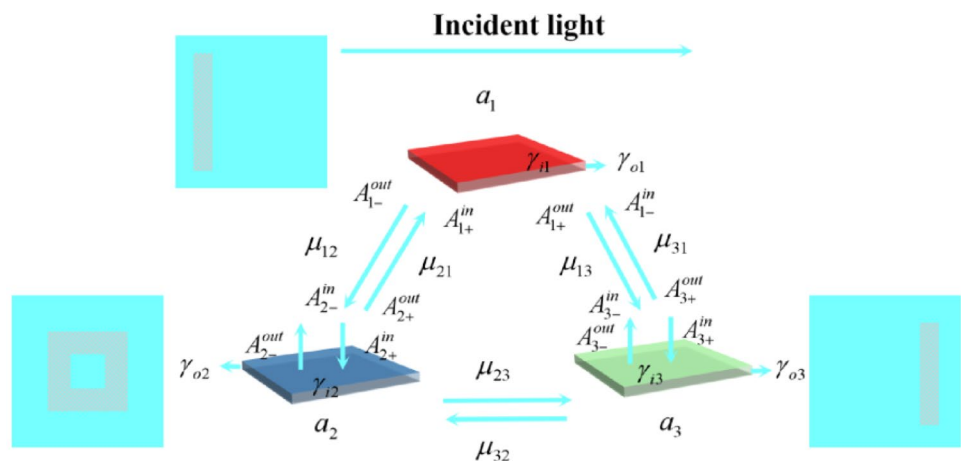
In order to better understand the principle behind PIT, we show the E_z of the electric field distribution of the structure at $f = 1.49$ THz, $f = 1.79$ THz and $f = 2.37$ THz in the graphene metamaterial structure, as shown in Fig. 3c-e. We observe that the electric fields are mainly concentrated at the edges of the L, R and M structures. Thus, direct coupling between different modes and incident light produces resonance at different frequencies.

To better understand how Fano resonance works, the coupled mode theory is employed, as shown in Fig. 4. A_1 , A_2 and A_3 which indicate three antennas that receive and transmit information are used to describe the coupling between different modes where “+” and “-” separately indicate the positive and negative directions of propagation along the antenna and “in” and “out” indicate, respectively, the states of inflow and outflow of incident light. $\gamma_{(i,n)}$ and $\gamma_{(o,n)}$ ($i = in, o = out, n = 1, 2, 3$) are the internal loss coefficient and external loss coefficient of the n th mode. μ_{mn} ($m = 1, 2, 3, m \neq n$) is the coupling coefficient between the three modes.

Therefore, the coupling between the three modes can be provided:

$$\begin{pmatrix} \gamma_1 & -i\mu_{12} & -i\mu_{13} \\ -i\mu_{21} & \gamma_2 & -i\mu_{23} \\ -i\mu_{31} & -i\mu_{32} & \gamma_3 \end{pmatrix} \cdot \begin{pmatrix} a_1 \\ a_2 \\ a_3 \end{pmatrix} = \begin{pmatrix} -\kappa_{(o,1)}^{-1/2} & 0 & 0 \\ 0 & -\kappa_{(o,2)}^{-1/2} & 0 \\ 0 & 0 & -\kappa_{(o,3)}^{-1/2} \end{pmatrix} \cdot \begin{pmatrix} A_{1+}^{in} + A_{1-}^{in} \\ A_{2+}^{in} + A_{2-}^{in} \\ A_{3+}^{in} + A_{3-}^{in} \end{pmatrix} \quad (3)$$

Fig. 4 Coupling model of three resonance modes



where, $\gamma_n = (i\omega - i\omega_n - \gamma_{(i,n)} - \gamma_{(o,n)})(n = 1, 2, 3)$, $\gamma_{(i,n)} = \omega_n / (2Q_{(i,n)})$ and $\gamma_{(o,n)} = \omega_n / (2Q_{(o,n)})$. a_1, a_2 and a_3 are the amplitudes of three resonators, respectively; μ_1, μ_2 and μ_3 are the coupling coefficients of three resonators, respectively; $Q_{(i,n)}$ is the

$$r = \frac{A_{-}^{in}}{A_{+}^{in}} = \kappa_{(o,1)}^{-1/2} e^{i(\varphi_1 + \varphi_2)} D_1 - \kappa_{(o,2)}^{-1/2} e^{i\varphi_2} D_2 - \kappa_{(o,3)}^{-1/2} D_3 \quad (8)$$

The coefficients in the formula are respectively[30]:

$$D_1 = \frac{(\gamma_2\gamma_3 - \gamma_{23}\gamma_{32})\gamma_{(o,1)}^{1/2} + (\gamma_{12}\gamma_3 + \gamma_{13}\gamma_{23})\gamma_{(o,2)}^{1/2} + (\gamma_{12}\gamma_{23} + \gamma_{13}\gamma_{23})\gamma_{(o,3)}^{1/2}}{\gamma_1\gamma_{23}\gamma_{32} - \gamma_1\gamma_2\gamma_3 + \gamma_{12}\gamma_{21}\gamma_3 + \gamma_{12}\gamma_{23}\gamma_{31} + \gamma_{13}\gamma_{21}\gamma_{32} + \gamma_{13}\gamma_2\gamma_{31}} \quad (9)$$

$$D_2 = \frac{(\gamma_{21}\gamma_3 - \gamma_{23}\gamma_{31})\gamma_{(o,1)}^{1/2} + (\gamma_1\gamma_3 + \gamma_{13}\gamma_{31})\gamma_{(o,2)}^{1/2} + (\gamma_1\gamma_{23} + \gamma_{13}\gamma_{21})\gamma_{(o,3)}^{1/2}}{\gamma_1\gamma_{23}\gamma_{32} - \gamma_1\gamma_2\gamma_3 + \gamma_{12}\gamma_{21}\gamma_3 + \gamma_{12}\gamma_{23}\gamma_{31} + \gamma_{13}\gamma_{21}\gamma_{32} + \gamma_{13}\gamma_2\gamma_{31}} \quad (10)$$

$$D_3 = \frac{(\gamma_{21}\gamma_{32} - \gamma_2\gamma_{31})\gamma_{(o,1)}^{1/2} + (\gamma_1\gamma_{32} + \gamma_{12}\gamma_{31})\gamma_{(o,2)}^{1/2} + (\gamma_1\gamma_2 + \gamma_{12}\gamma_{21})\gamma_{(o,3)}^{1/2}}{\gamma_1\gamma_{23}\gamma_{32} - \gamma_1\gamma_2\gamma_3 + \gamma_{12}\gamma_{21}\gamma_3 + \gamma_{12}\gamma_{23}\gamma_{31} + \gamma_{13}\gamma_{21}\gamma_{32} + \gamma_{13}\gamma_2\gamma_{31}} \quad (11)$$

$$\gamma_{12} = i\mu_{12} + (\gamma_{(o,1)}\gamma_{(o,2)})^{1/2}, \gamma_{13} = i\mu_{13} + (\gamma_{(o,1)}\gamma_{(o,3)})^{1/2}, \gamma_{21} = i\mu_{21} + (\gamma_{(o,1)}\gamma_{(o,2)})^{1/2} \quad (12)$$

$$\gamma_{23} = i\mu_{23} + (\gamma_{(o,2)}\gamma_{(o,3)})^{1/2}, \gamma_{31} = i\mu_{31} + (\gamma_{(o,1)}\gamma_{(o,3)})^{1/2}, \gamma_{32} = i\mu_{32} + (\gamma_{(o,2)}\gamma_{(o,3)})^{1/2} \quad (13)$$

internal loss coefficient, $Q_{(o,n)}$ is the external loss coefficient. The $Q_{(i,n)}$ and $Q_{(o,n)}$ satisfy $1/Q_{(i,n)} = 1/Q_{(i,n)} + 1/Q_{(o,n)}$. In this formula, $Q_{(i,n)}$ is the quality factor of the n th hypothetical resonator, $Q_m = f/df$. ω_n is the angular frequency of the n th modes. According to the law of conservation of energy, when the incident light enters resonator L on its way through resonator M and finally comes out of resonator R, we can obtain the relationships between the three coupled modes:

$$A_{n+}^{in} = A_{(n-1)+}^{out} e^{i\varphi_{n-1}}, A_{(n-1)-}^{in} = A_{n-}^{out} e^{i\varphi_{n-1}} (n = 2, 3) \quad (4)$$

$$A_{n+}^{out} = A_{n+}^{in} - \kappa_{(o,n)}^{-1/2} a_n, A_{n-}^{out} = A_{n-}^{in} - \kappa_{(o,n)}^{-1/2} a_n (1, 2, 3) \quad (5)$$

$$A_{3-}^{in} = 0 \quad (6)$$

where, φ_1 is the phase difference between two modes A_1 and A_2 , φ_2 is the phase difference between two modes A_2 and A_3 . However, the rationalization in the study assumes that the three antennas are in the same plane because the thickness of the oxide layer has little effect on the transmission spectrum of the structure, the phase difference is zero when a beam of linearly polarized plane light is incident vertically. To sum up, the transmission and reflection coefficients of the system are obtained:

$$t = \frac{A_{3+}^{out}}{A_{1+}^{in}} = 1 - \kappa_{(o,1)}^{-1/2} e^{i(\varphi_1 + \varphi_2)} D_1 - \kappa_{(o,2)}^{-1/2} e^{i\varphi_2} D_2 - \kappa_{(o,3)}^{-1/2} D_3 \quad (7)$$

Therefore, the transmission spectrum, reflection spectrum and absorption spectrum of the whole system are

$$T = t^2 = \frac{r_d^2(\omega - \omega_0)^2 + t_d^2\gamma^2 \mp 2r_d t_d(\omega - \omega_0)\gamma}{(\omega - \omega_0)^2 + \gamma^2},$$

$$R = r^2 = \frac{t_d^2(\omega - \omega_0)^2 + r_d^2\gamma^2 \pm 2r_d t_d(\omega - \omega_0)\gamma}{(\omega - \omega_0)^2 + \gamma^2}, \quad (14)$$

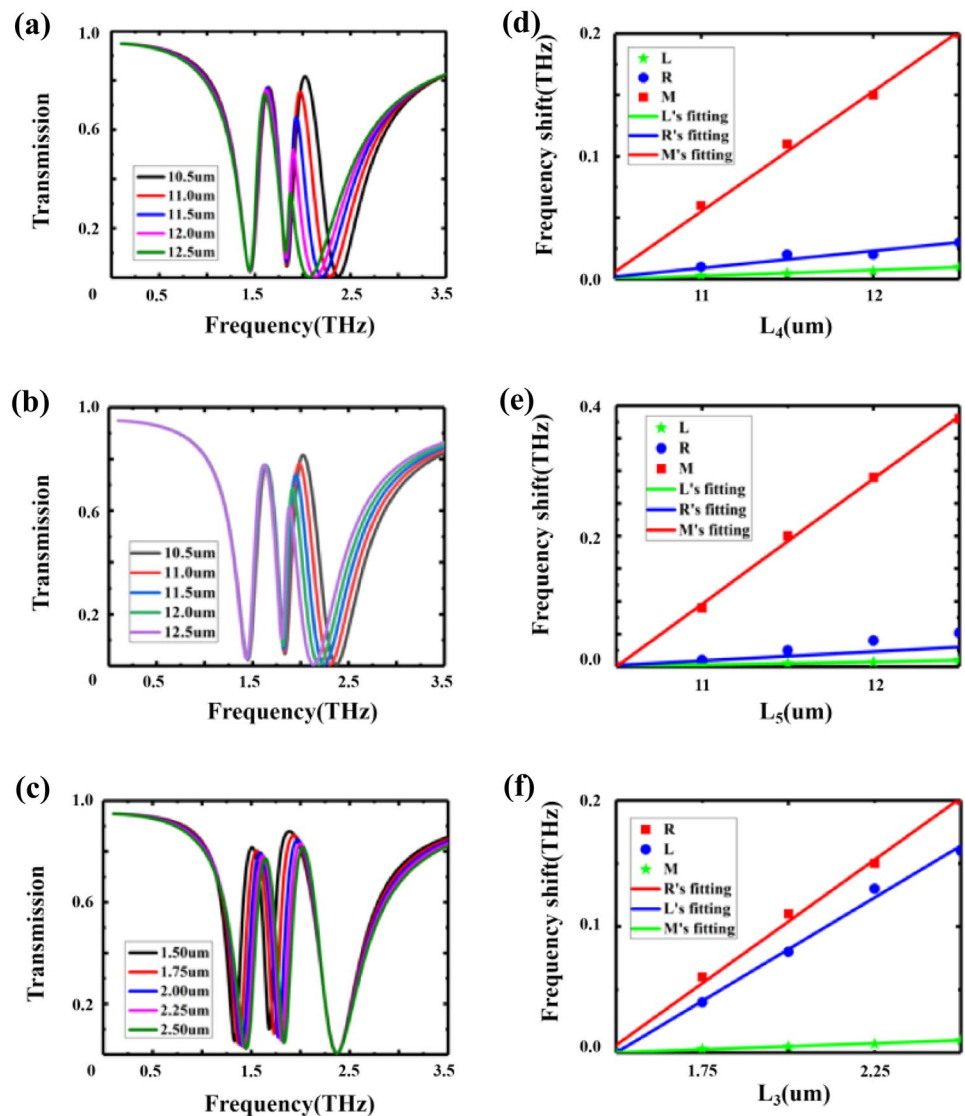
$$A = 1 - T - R$$

where, t_d is transmission coefficient, r_d is the direct reflection which satisfies, ω is frequency, ω_0 is the resonance frequency, γ is the radiation rate of the mode.

In Fig. 5, on account of the electric field enhancement effect for particle adsorption mode, we explore the curve evolution of PIT by changing the geometric parameters of the graphene structure. With the increase of longitudinal length L_4 and crosswave length L_5 of the lower layer of square ring graphene, as shown in Fig. 5a, b, we can clearly observe that the third transmission spectrum of the PIT curve has an obvious red-shift. Simultaneously, the first and second transmission spectrum of the PIT curve also show an obvious red-shift with the increase of crosswave length L_3 of the upper graphene band, as shown in Fig. 5c. The frequency shift is mainly due to the significant influence of the great overlay between the graphene strips and the graphene rings.

In addition, we discuss the potential of the higher order plasma mode with a bilayer graphene structure in terahertz

Fig. 5 Evolution of the PIT curve when the longitudinal length L_4 (a) and the longitudinal length L_5 (b) of the lower layer of square ring graphene and the crosswave length L_3 (c) of upper graphene band; (d-f) Frequency shifts of three resonant frequencies versus changes the geometric parameters of the graphene structure



sensing applications. The absorption spectra of bilayer graphene structures embedded in different ambient media are calculated with the same geometric parameters as shown

in Fig. 1b. We plot the frequency shifts of three resonant frequencies with respect to changing the design value of the graphene structure, as shown in Fig. 5d-f. We observe that

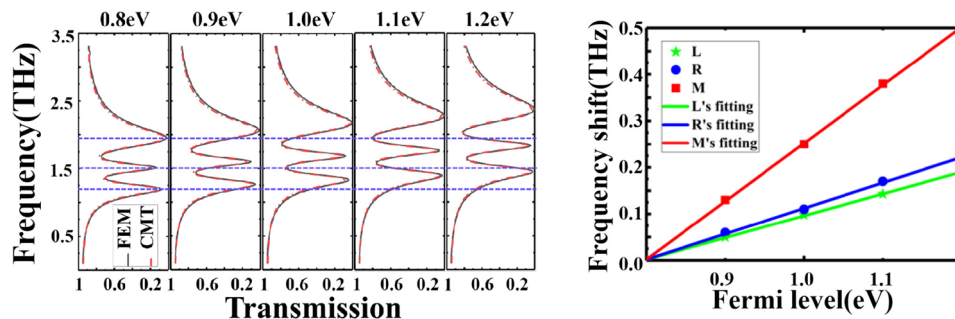


Fig. 6 a The PIT transmission spectra of numerical simulation and fitting at the different Fermi levels of graphene. b Frequency shifts of three resonant frequencies versus Fermi level. We define $S(S=\Delta f/\Delta E_f)$ as the linear fitting sensitivity. Here, Δf and ΔE_f are the change

in frequency shift and the change in Fermi level respectively. CMT and FEM are shorthand for coupled mode theory and finite element method, respectively

Table 1 Comparison of the proposed structure with previously reported structures

| Sensor | Sensitivity | FOM |
|--------------------|--------------------|------------------------|
| Ref [31] | $S=0.36$ THz/RIU | FOM=0.97 |
| Ref [32] | $S=0.44$ THz/RIU | FOM=2.93 |
| Ref [33] | $S=0.53$ THz/RIU | FOM=5.39 |
| Ref [34] | $S=0.59$ THz/RIU | FOM=4.53 |
| Proposed structure | $S_1=1.95$ GHz/meV | FOM ₁ =7.8 |
| | $S_2=2.21$ GHz/meV | FOM ₂ =12.2 |
| | $S_3=5.00$ GHz/meV | FOM ₃ =9.43 |

the resonance frequency also changes linearly as the structural parameters of graphene change linearly. Therefore, the double-layer graphene structure we designed can be used in the field of sensors illustriously.

The PIT transmission spectra of the numerical simulation are fitted by CMT, as shown in Fig. 6a. It can be seen that the CMT theoretical calculation results of the proposed structure agree well with the finite element simulation results. We can also perceive that the PIT curve has an obvious blue-shift with the increase of the Fermi level which can manifest superior modulation function of the bilayer graphene structure. In the scope of 0.8 eV to 1.2 eV, the extinction ratio of the third transmission spectrum can be up to 100% which means that it can carry out an excellent single-band filter. We define $S(S = \Delta f / \Delta E_f)$ as the linear fitting sensitivity. Here, Δf and ΔE_f are the change in frequency shift and the change in Fermi level respectively. Using Fig. 6b, we figured out the high Fermi level sensitivities of $S_1 = 1.95$ GHz/meV, $S_2 = 2.21$ GHz/meV and $S_3 = 5.00$ GHz/meV. Here, S_1 , S_2 and S_3 represent the sensitivities of transmission at three resonant frequencies, respectively. These amounts are much higher than previous studies in related field [31–34]. The sensitivities of the structures mentioned above are compared with our structure in Table 1.

In addition, we further quantify the figure of merit (FOM), which is defined as sensitivity divided by FWHM [35, 36]. The FOMs of the proposed bilayer graphene structure at the three resonant frequencies in the terahertz range are 7.8, 12.2 and 9.43 that are three to four times higher compared to 2.93 in Ref [32]. and 4.53 in Ref. [34], respectively, providing a practical application for terahertz refractive index sensing.

Meanwhile, electro-optical switch can be implemented based on the PIT effect at the frequency of 2.0 THz, as shown in Fig. 7a. As we all know, modulation degree (MD) can be signified by $(T-D)/T \times 100\%$ where T is the maximum transmittance, and D is the minimum transmittance. Even more noteworthy is that the mobility of graphene observed from the experimental data is essentially independent of temperature. Because of this we can attest that the mobility of graphene is still limited by impurity scattering at 300 K. By applying the gate voltage, we observed carrier concentrations in graphene as high as $4 \times 10^8 \text{ m}^{-2}$, which means $E_f = 1.17 \text{ eV}$ [37, 38]. Therefore, it is

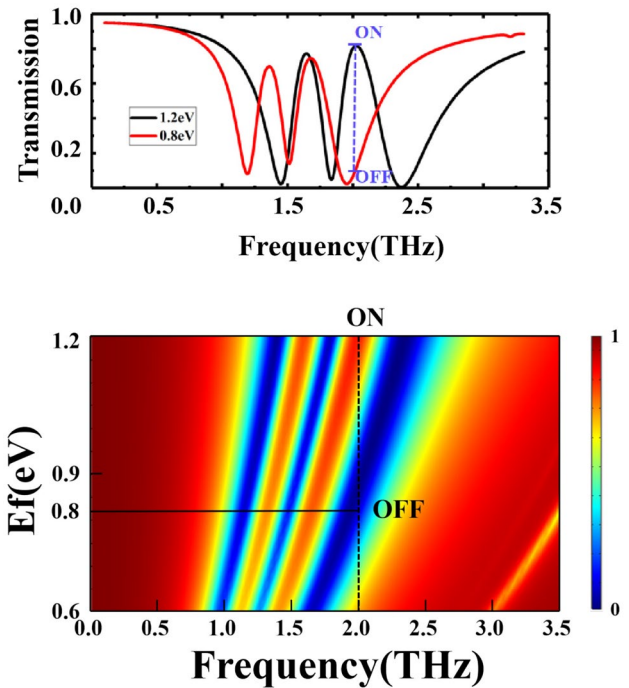


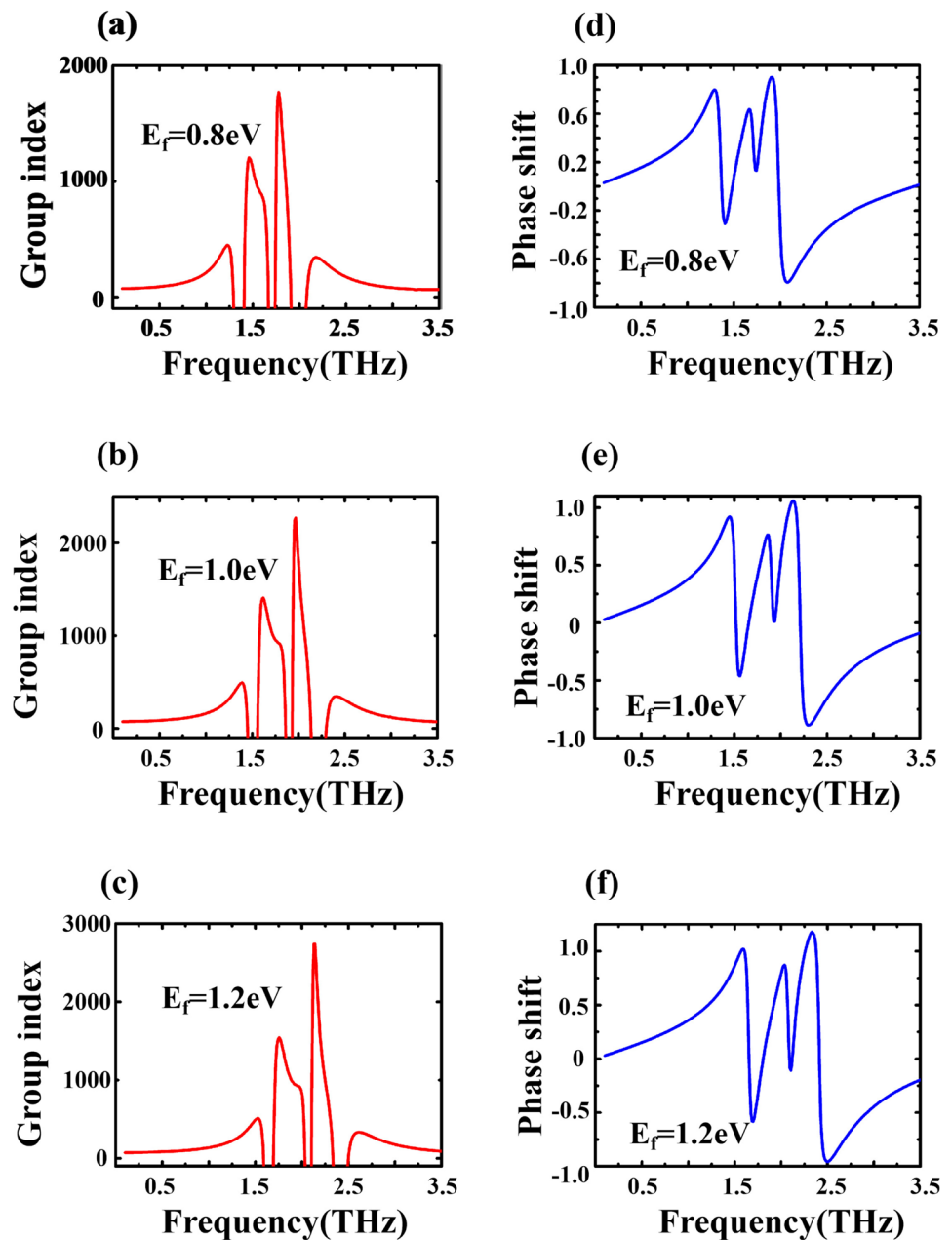
Fig. 7 a Modulation mechanism of electro-optical switch; b Three-dimensional modulation diagram at different graphene Fermi levels. ON and OFF are abbreviations for the on and off state of the photoelectric switch, respectively

reasonable to assume that the Fermi level may be dynamically modulated from 0.8 eV to 1.2 eV in the PIT system.

Through the above research, the MD of amplitude at 2.0 THz is 99.63% where transmission is 86% in 2.0 THz and D is 6% in 2.0 THz, which means that the on–off modulation can be enforced. Hence the "on" state is set to the transmission rate of 86%, and the "off" state is set to the transmission rate of 6%. Figure 7b shows a three-dimensional modulation diagram that reflects the mechanism of the on–off switch.

An important area of PIT application is slow light effect. Here we analyze the slow light properties of the proposed metamaterial structures in Fig. 8. Generally speaking, the size of group index determines the quality of slow light effect, the larger the group index, the better the slow light characteristics. It can be obtained by: $n_g = c \cdot dk = c \cdot d\theta / (l \cdot d\omega)$ [39], where c , k , l are the light velocity, the wave vector in vacuum and the thickness of the substrate SiO_2 , respectively, and transmission phase shift is $\theta = \arg(t)$. Therefore, we plot the group index and phase shift at transparent windows from 0.8 eV to 1.2 eV in Fig. 8, the max group index of the metamaterials increases with increasing of the Fermi level. When Fermi energy level is 1.2 eV, the group index can be as high as 2739. Because of the sharp change of phase shift at the resonant frequency, the group exponent decreases sharply. Thence, there is a large group index near the resonant frequency caused by strong dispersion. Therefore, we can effectively adjust the double PIT phenomenon to seek the ideal slow light effect.

Fig. 8 a-c Group index of the proposed metamaterials at different Fermi Levels; d-f Phase shifts of the proposed metamaterials at different Fermi levels



Conclusions

From what has been discussed above, with two graphene bands of different lengths on the upper layer and a square ring on the lower layer, we design a two-layer graphene absorber on a SiO_2 substrate. The structure is numerically calculated by the finite element method and coupled with the simulation results by coupling mode theory. Through simulation, it can be found that the three resonant frequencies of the PIT transmission spectrum obtained can be changed by changing linearly the structural parameters. We also obtain the linear relationship between the frequency shift of the three resonant frequencies of the PIT

transmission spectrum and the Fermi level change, and the linear fitting sensitivity of the three resonant frequencies is $S_1 = 1.95 \text{ GHz/meV}$ and $S_2 = 2.21 \text{ GHz/meV}$ and $S_3 = 5.00 \text{ GHz/meV}$, respectively, and FOMs are 7.8, 12.2 and 9.43. Meanwhile, an electro-optical switch can be implemented based on the PIT effect at a frequency of 2.1 THz, where the MD of amplitude at 2.1 THz is 99.63%. In addition, the slow-light characteristics of the proposed structure are very outstanding, and the group index is as high as 2739. Through the above research, the structure designed by us can be applied to light switches, absorbers, refractive index sensing and other fields.

Authors' Contributions Conceptualization, J.Z. and J.W.; methodology, Z.D.H. and J.W.; software, J.Z. and Y.C.; validation, Y.C. and B.Z.; formal analysis, Z.B, Z.D.H., J.W.; writing—original draft preparation, J.Z., J.W.; writing—review and editing, Z.D.H., B.Z., and J.W.; visualization, Z.D.H.; supervision, J.W.; project administration, J.W., Z.D.H.; funding acquisition, J.W., Z.D.H. All authors have read and agreed to the published version of the manuscript.

Fundings This work is supported by the National Natural Science Foundation of China (11,811,530,052), the Intergovernmental Science and Technology Regular Meeting Exchange Project of the Ministry of Science and Technology of China (CB02-20), the Open Fund of State Key Laboratory of Applied Optics (SKLAO2020001A04), the Open Fund of CAS Key Laboratory of Quantum Information (KQI201), and the Undergraduate Research and Innovation Projects of China (2021102Z).

Availability of Data and Material All data that support the findings of this study are included within the article.

Code Availability The code that support the findings of this study are available from the corresponding author upon reasonable request.

Declarations

Competing interests The authors declare no competing interests.

Consent to Participate The authors declare that they have no conflicts of interest

Consent for Publication The authors grant the Publisher the sole and exclusive license of the full copyright in the Contribution, which license the Publisher hereby accepts. Consequently, the Publisher shall have the exclusive right throughout the world to publish and sell the Contribution in all languages, in whole or in part, including, without limitation, any abridgement and substantial part thereof, in book form and in any other form including, without limitation, mechanical, digital, electronic and visual reproduction, electronic storage and retrieval systems, including internet and intranet delivery and all other forms of electronic publication now known or hereinafter invented.

Conflicts of interest The authors declare no conflict of interest.

References

- Shelby AR (2001) Experimental verification of a negative index of refraction. *Science* 292:77–79
- Schurig D, Mock JJ, Justice BJ, Cummer SA, Pendry JB, Starr AF, Smith DR (2006) Metamaterial electromagnetic cloak at microwave frequencies. *Science* 314:977–980
- Pendry JB (2000) Negative refraction makes a perfect lens. *Phys Rev Lett* 85:3966–3969
- Zhang YB, Tang TT, Girit C, Hao Z, Martin MC, Zettl A, Crommie MF, Shen YR, Wang F (2009) Direct observation of a widely tunable bandgap in bilayer graphene. *Nature* 459:820–823
- Bao Z, Wang J, Hu ZD, Balmakou A, Khakhomov S, Tang Y, Zhang C (2019) Coordinated multi-band angle insensitive selection absorber based on graphene metamaterials. *Opt Express* 27(22):31435–31445
- Bao Z, Tang Y, Hu ZD, Zhang C, Balmakou A, Khakhomov S, Semchenko I, Wang J (2020) Inversion method characterization of graphene-based coordination absorbers incorporating periodically patterned metal ring metasurfaces. *Nanomaterials* 10(6):1102
- Wang S, Ang PK, Wang Z, Tang ALL, Thong JTL, Loh KP (2010) High Mobility, Printable and solution-processed graphene electronics. *Nano Letters* 10(1):92–98
- Wang JC, Wang XS, Hu ZD, Zheng GG, Zhang F (2017) Peak modulation in multi-cavity-coupled graphene-based waveguide system. *Nanoscale Res Lett* 12:9
- Vakil A, Engheta N (2011) Transformation optics using graphene. *Science* 332(6035):1291–1294
- Zhang Y, Brar VW, Wang F, Girit C, Yayan Y, Panlasigui M, Zettl A, Crommie MF (2008) Giant phonon-induced conductance in scanning tunnelling spectroscopy of gate-tunable graphene. *Nat Phys* 4(8):627–630
- Jia W, Ren P, Jia Y, Fan C (2019) Active control and large group delay in graphene-based terahertz metamaterials. *J Phys Chem C* 123(30):18560–18564
- Ju L, Geng B, Horng J, Girit C, Martin M, Hao Z, Bechtel HA, Liang X, Zettl A, Shen YR, Wang F (2010) Graphene plasmonics for tunable terahertz metamaterials. *Nat Nanotechnol* 6(10):630–634
- Low T, Avouris P (2014) Graphene plasmonics for terahertz to mid-Infrared applications. *ACS Nano* 8(2):1086–1101
- Shi WJ, Wang YQ, Zhou JC, Hu ZD, Wang JC, Hu LF (2021) Multifunctional Fano resonance modulator with graphene-based double-layer independent gratings. *J Opt Soc Am B* 38(10):2823–2829
- Song MW, Wang CT, Zhao ZY, Pu MB, Liu L, Zhang W, Yu HL, Luo XG (2016) Nanofocusing beyond the near-field diffraction limit via plasmonic Fano resonance. *Nanoscale* 8:3
- Luo X, Cheng ZQ, Zhai X, Liu ZM, Li SQ, Liu JP, Wang LL, Lin Q, Zhou YH (2019) A tunable dual-band and polarization-insensitive coherent perfect absorber based on double-layers graphene hybrid waveguide. *Nanoscale Res Lett* 14:337
- Gao E, Liu Z, Li H, Xu H, Zhang Z, Luo X, Xiong C, Liu C, Zhang B, Zhou F (2019) Dynamically tunable dual plasmon-induced transparency and absorption based on a singlelayer patterned graphene metamaterial. *Opt Express* 27:13884–13894
- Wang J, Song C, Hang J, Hu Z, Zhang F (2017) Tunable fano resonance based on grating-coupled and graphene-based otto configuration. *Opt Express* 27:13884
- Zhang S, Genov DA, Wang Y, Liu M, Zhang X (2008) Plasmon-induced transparency in metamaterials. *Phys Rev Lett* 101(4):047401
- Khazaei S, Granpayeh N (2018) Tunable multiple plasmon induced transparencies in parallel graphene sheets and its applications. *Optics Communications* 406:199–204
- Zeng C, Cui Y, Liu X (2015) Tunable multiple phase-coupled plasmon-induced transparencies in graphene metamaterials. *Opt Express* 23(1):545–551
- Chen X, Fan W (2016) Polarization-insensitive tunable multiple electromagnetically induced transparencies analogue in terahertz graphene metamaterial. *Opt Mater Express* 6(8):2607–2615
- Xu H, Li H, He Z, Chen Z, Zheng M, Zhao M (2017) Dual tunable plasmon-induced transparency based on silicon-air grating coupled graphene structure in terahertz metamaterial. *Opt Express* 25(17):20780–20790
- Gan CH, Chu HS, Li EP (2012) Synthesis of highly confined surface plasmon modes with doped graphene sheets in the mid-infrared and terahertz frequencies. *Phys Rev B* 85:117–122
- Du W, Li K, Wu D, Jiao K, Jiao L, Liu L, Xia F, Kong W, Dong L, Yun M (2019) Electrically controllable directional coupler based on tunable hybrid graphene nanoplasmonic waveguide. *Opt Commun* 430:450–455
- Chen JH, Jang C, Xiao S, Ishigami M, Fuhrer MS (2008) Intrinsic and extrinsic performance limits of graphene devices on SiO₂. *Nat Nanotechnol* 3(4):206–209
- Zhang J, Zhu Z, Liu W, Yuan X, Qin S (2015) Towards photo-detection with high efficiency and tunable spectral selectivity:

- graphene plasmonics for light trapping and absorption engineering. *Nanoscale* 7(32):13530–13536
28. Wu D, Wang M, Feng H, Xu Z, Liu Y, Xia F, Zhang K, Kong W, Dong L, Yun M (2019) Independently tunable perfect absorber based on the plasmonic properties in double-layer graphene. *Carbon* 155:618–623
 29. Islam MS, Sultana J, Biabanifard M, Vafapour Z, Nine MJ, Dinovitser A, Cordeiro CMB, Ng BW-H, Abbott D (2020) Tunable localized surface plasmon graphene metasurface for multiband superabsorption and terahertz sensing. *Carbon* 158:559–567
 30. Gao ED, Liu ZM, Li HJ, Xu H, Zhang ZB, Lu X, Xiong CX, Liu C, Zhang BH, Zhou FQ (2019) Dynamically tunable dual plasmon-induced transparency and absorption based on a single-layer patterned graphene metamaterial. *Opt Express* 27(10):13884–13894
 31. Tang P, Li J, Du L, Liu Q, Peng Q, Zhao J, Zhu B, Li Z, Zhu L (2018) Ultrasensitive specific terahertz sensor based on tunable plasmon induced transparency of a graphene micro-ribbon array structure. *Opt Express* 26(23):30655–30666
 32. Liu C, Liu P, Yang C, Lin Y, Zha S (2018) Dynamic electromagnetically induced transparency based on a metal-graphene hybrid metamaterial. *Optical Material Express* 8(5):1132–1142
 33. Hu S, Liu D, Yang H, Wang H, Wang Y (2019) Staggered H-shaped metamaterial based on electromagnetically induced transparency effect and its refractive index sensing performance. *Opt Commun* 450:202–207
 34. Zhang H, Cao Y, Liu Y, Li Y, Zhang Y (2017) A novel graphene metamaterial design for tunable terahertz plasmon induced transparency by two bright mode coupling. *Opt Commun* 391:9–15
 35. Azzam SI, Kildishev AV, Ma RM, Ning CZ, Oulton R, Shalaev VR, Stockman MI, Xu JL, Zhang X (2020) Ten years of spasers and plasmonic nanolasers. *Light Sci Appl* 9:90
 36. Skalsky S, Zhang Y, Alanis JA, Fonseca HA, Sanchez AM, Liu H, Parkinson P (2020) Heterostructure and Q-factor engineering for low-threshold and persistent nanowire lasing. *Light Sci Appl* 9:43
 37. Efetov DK, Kim P (2010) Controlling electron-phonon interactions in graphene at ultrahigh carrier densities. *Phys Rev Lett* 105:256805
 38. Balci S, Balci O, Kakenov N, Atar FB, Kocabas C (2016) Dynamic tuning of plasmon resonance in the visible using graphene. *Opt Lett* 41:1241
 39. Zentgraf T, Zhang S, Oulton RF, Zhang X (2009) Ultranarrow coupling-induced transparency bands in hybrid plasmonic systems. *Phys Rev B* 80(19):195415
- Publisher's Note** Springer Nature remains neutral with regard to jurisdictional claims in published maps and institutional affiliations.